Photoemission properties of quasi-one-dimensional conductors

2006 J. Phys.: Condens. Matter 18 3655

(http://iopscience.iop.org/0953-8984/18/15/012)

INSTITUTE OF PHYSICS PUBLISHING JOURNAL OF PHYSICS: CONDENSED MATTER

J. Phys.: Condens. Matter **18** (2006) 3655–3670 doi:10.1088/0953-8984/18/15/012

Photoemission properties of quasi-one-dimensional conductors

Ž Bonačić Lošić[1], P Županović[1] and A Bjeliš[2]

[1] Department of Physics, Faculty of Natural Sciences, Mathematics and Education, University of Split, Teslina 12, 21000 Split, Croatia
[2] Department of Physics, Faculty of Science, University of Zagreb, POB 162, 10001 Zagreb, Croatia

E-mail: agicz@pmfst.hr and bjelis@phy.hr

Received 25 July 2005, in final form 27 February 2006
Published 30 March 2006
Online at stacks.iop.org/JPhysCM/18/3655

Abstract

We calculate the one-particle spectral function and the corresponding derived quantities for a chain lattice with a one-dimensional conducting electron band, and with a three-dimensional long-range Coulomb electron–electron interaction treated within the G_0W_0 approximation. It is shown that due to the anisotropic acoustic dispersion of the plasmon mode, the quasi-particle peak as a standard Fermi liquid feature does not show up in the spectral function. Instead, the latter comprises only a broad maximum with width of the order of plasmon energy. Such spectral properties are in the qualitative agreement with ARPES spectra of Bechgaard salts obtained in recent measurements. The present approach is appropriate for the treatment of wide energy scales defined by the width of the conducting band and the plasmon energy, and is complementary to earlier rigorous results obtained within the Luttinger liquid approach in the asymptotic limit of low energies close to the chemical potential.

1. Introduction

Spectral properties of the quasi-one-dimensional conductors in the metallic state are in many respects different from those of standard three-dimensional metals. The latter are theoretically covered by the Landau theory of Fermi Liquids, usually extended by the random phase approximation (RPA) treatment of the long-range electron–electron Coulomb interaction. The central prediction of this theory is the appearance of quasi-particle peaks in the spectral function at energies close to the chemical potential and wavevectors close to the Fermi wavevector [1]. Furthermore, due to these peaks the momentum distribution function shows a discontinuity at the Fermi wavevector [2, 3].

The Fermi liquid approach is however inadequate for the treatment of the anomalous behaviour of particle–hole and/or particle–particle correlations in the quasi-one-dimensional

conductors belonging to the class of Luttinger liquids. This is shown within various non-perturbational approaches, particularly those using the renormalization group and bosonization techniques. Calculations of one-particle propagator within these approaches show that the energy dependence of the density of states close to the chemical potential is given by the power law $N(\omega) \sim |\omega|^{\alpha}$, where α is the interaction-dependent anomalous dimension [4]. The frequency dependence of the corresponding one-particle spectral function at the Fermi wavenumber obtained for the spinfull spin-rotation-invariant Luttinger model is $A(k_{\mathrm{F}}, \omega) \sim |\omega|^{\alpha-1}$, showing that the spectral weight moves away from the Fermi energy as α exceeds unity [4]. The corresponding momentum distribution function is continuous at the Fermi wavenumber.

The ARPES spectra of the Bechgaard salts $(TMTSF)_2X$ PF_6 where TMTSF stands for tetramethyltetraselenafulvalene and $X = PF_6, AsF_6, ClO_4, \ldots$ [5–7] show a broad maximum at energies of the order of the plasmon collective mode and a disappearance of the spectral weight at the chemical potential. This seems to be in qualitative agreement with the Luttinger liquid picture, although there are some indications, for example the insensitivity of the almost linear tail disappearing at the chemical potential on the wavevector, that the main properties of the spectra could originate from surface effects [8]. As for the interpretation within the Luttinger liquid approach, it is consistent provided the value of α for investigated salts is larger than unity. Such a regime of values for α is realized in systems with strong enough long-range Coulomb interaction (including electron–electron interaction between neighbouring sites) [9–12], and is to be contrasted with the regime $\alpha \leqslant 1/8$ characterizing Luttinger liquids with a dominant on-site Hubbard interaction.

The above estimation of the value of the anomalous dimension places the value of the 'charge stiffness constant' K_ρ, connected with α through the relation $\alpha = (K_\rho + K_\rho^{-1} - 2)/4$, in the range $K_\rho < 0.17$, which agrees with some, but not all, other independent measurements. For example, the temperature dependence of the spin–lattice relaxation rate T_1^{-1} has exponent $K_\rho \approx 0.1$ [13, 14], which implies $\alpha \approx 2$, consistent with photoemission experiments, while, on the other hand, optical conductivity and resistivity measurements suggest much larger values of K_ρ, namely 0.23 [7, 15, 16] and 0.25 [17, 18] respectively.

The spectral properties at energies of the order of the plasmon and/or bandwidth energy become particularly interesting due to the already mentioned unusual experimental photoemission data, although, again, the corresponding large energy ranges of 1 eV can be affected by surface contributions as well. From the microscopic point of view this energy range is out of the scope of methods used in the treatments of Luttinger liquids which are limited to the low-energy regime. In the present paper we investigate this range by applying the standard so-called G_0W_0 approximation in the calculation of the dressed electron Green's function. More precisely, we analyse the spectral properties of the quasi-one-dimensional metal with a rectangular lattice of parallel chains, paying particular attention to the long-range Coulomb interaction, which, as indicated above, plays a crucial role in the photoemission properties of Bechgaard salts. More specifically, we take into account the three-dimensional Coulomb interaction between conducting electrons, and assume a strictly one-dimensional electron band due to a finite transfer integral along the chains. The extension to the more realistic case of electron bands with a finite transverse dispersion is preliminary considered in [19]. The full discussion will be given elsewhere [20].

The present approximation for the electron Green's function was used previously by Hedin and Lundqvist in the calculation of the spectral function for the three-dimensional 'jellium' model [21–23]. It was found that the spectral density is mainly determined by the plasmon mode. More precisely, $A(k_{\mathrm{F}}, \omega)$ has a finite weight in the energy range of the order of the long-wavelength plasmon energy Ω_{pl}, and the quasi-particle peak with a reduced spectral weight in

the energy range $\mu - \Omega_{\rm pl} < \omega < \mu + \Omega_{\rm pl}$. In other words, the plasmon mode causes a transfer of a significant part of the quasi-particle peak weight into the plasmon energy ranges above and below the Fermi energy. Still, the quasi-particle exists, in agreement with the expectation that the Landau theory of Fermi Liquids applies to the three-dimensional 'jellium'.

It is worthwhile warning here that the G_0W_0 approximation generally does not lead to a fully self-consistent result regarding the position of the chemical potential in the homogeneous electron gas [24], and particularly in inhomogeneous systems [25]. This problem is usually addressed by introducing a shift of the chemical potential entering through the self-energy already in the bare Green's function, in a way that it self-consistently coincides with the position of the chemical potential in the final dressed Green's function [25, 26]. We shall adopt this procedure accordingly in the present treatment.

The particular property of the plasmon mode in our case of strictly one-dimensional electron band is its anisotropic acoustic dispersion in the long-wavelength limit. Since the collective plasmon excitations now cover the whole range of energies, including that of the quasi-particle excitations in the three-dimensional 'jellium', the question arises whether the quasi-particle will appear at all in the spectral density. The present calculations will show that, provided that there is no transverse interchain hopping of electrons, the spectral density is indeed dominated by a broad feature with width of the order of the plasmon energy.

In section 2 we develop the G_0W_0 method for the calculation of the electron self-energy due to the RPA screened Coulomb interaction, and compare the obtained real and imaginary part of reciprocal Green's function with the corresponding results of the three-dimensional isotropic 'jellium'. In sections 3 and 4 we analyse the obtained one-particle spectral function, as well as the other quantities derived from it like the density of states and the momentum distribution function, and show that the obtained spectral properties are in a qualitative agreement with the ARPES spectra of the Bechgaard salts. Section 5 summarizes the main results.

2. Green's function

2.1. Dyson equation

We start with the G_0W_0 approximation for the electron self-energy, with the RPA screened Coulomb interaction playing the role of effective potential. The Dyson equation for the one-particle Green's function in the $(\mathbf{r}, \omega)$-space is given by

$$\begin{aligned} G(\mathbf{r}, \mathbf{r}', \omega) = G_0(\mathbf{r}, \mathbf{r}', \omega) + \frac{\mathrm{i}}{2\pi} \int G_0(\mathbf{r}, \mathbf{r}_1, \omega) G_{0s}(\mathbf{r}_1, \mathbf{r}_1', \omega') \\ \times V(\mathbf{r}_1, \mathbf{r}_1') \mathrm{e}^{\mathrm{i}\omega'\delta} G(\mathbf{r}_1', \mathbf{r}', \omega)\, \mathrm{d}\mathbf{r}_1\, \mathrm{d}\mathbf{r}_1'\, \mathrm{d}\omega' + \frac{\mathrm{i}}{2\pi} \int G_0(\mathbf{r}, \mathbf{r}_1, \omega) G_{0s}(\mathbf{r}_1, \mathbf{r}_1', \omega') \\ \times [\bar{V}(\mathbf{r}_1, \mathbf{r}_1', \omega - \omega') - V(\mathbf{r}_1, \mathbf{r}_1')] G(\mathbf{r}_1', \mathbf{r}', \omega)\, \mathrm{d}\mathbf{r}_1\, \mathrm{d}\mathbf{r}_1'\, \mathrm{d}\omega' \end{aligned} \tag{1}$$

where $V(\mathbf{r}_1, \mathbf{r}_1')$ and $\bar{V}(\mathbf{r}_1, \mathbf{r}_1', \omega')$ are the bare interaction and the RPA screened interaction respectively. In equation (1) we separate the exchange contribution from the contribution comprising only the sum of the RPA bubble diagrams without the bare Coulomb interaction, given by second term and third term, respectively. Since the fermion line in the time-dependent version of the exchange contribution begins and ends at the same time, i.e. the corresponding time difference is infinitesimally small, the exchange term in the frequency representation of equation (1) carries the phase factor $\mathrm{e}^{\mathrm{i}\omega'\delta}$, $\delta \to 0^+$ (see e.g. [1, 27, 28]). This is not the case with the diagrams from the third term in equation (1) in which the time difference between end points of the fermion line is finite. Having in mind the remarks from section 1 on the

inconsistency of the G_0W_0 approximation regarding the non-conservation of the fermions, we follow the procedure proposed by Hedin [26] and elaborated by Schindlmayr [25], and introduce in equation (1) the bare Green's function G_{0s} with a shifted chemical potential,

$$G_{0s}(k_\parallel, \omega) = \frac{1 - n(k_\parallel)}{\omega - E_0(k_\parallel) - \mu + \mathrm{i}\eta} + \frac{n(k_\parallel)}{\omega - E_0(k_\parallel) - \mu - \mathrm{i}\eta}. \tag{2}$$

The shift μ with respect to the chemical potential of the Green's function for the non-interacting fermions $G_0(k_\parallel, \omega)$ (chosen conventionally to be zero, as is seen below from equations (4), (9)) will be determined self-consistently from the requirement that it coincides with the chemical potential of the dressed Green's function $G(k_\parallel, \omega)$.

In the $(\mathbf{q}, \omega)$-space the Dyson equation reads

$$G^{-1}(\mathbf{k}, \omega) = G_0^{-1}(k_\parallel, \omega) - \frac{\mathrm{i}}{2\pi N} \sum_{\mathbf{q}} \left\{ \int \mathrm{d}\omega' \, G_{0s}(q_\parallel, \omega') V(\mathbf{k} - \mathbf{q}) \mathrm{e}^{\mathrm{i}\omega'\delta} + \int \mathrm{d}\omega' \, G_{0s}(q_\parallel, \omega') [\bar{V}(\mathbf{k} - \mathbf{q}, \omega - \omega') - V(\mathbf{k} - \mathbf{q})] \right\}, \tag{3}$$

with the exchange contribution separated from the rest of the self-energy like in equation (1). Since it is assumed that the electrons propagate only along chains, the electron dispersion depends only on the longitudinal component of the wavevector $k_\parallel$. More specifically, the tight-binding single-particle energy spectrum is given by

$$E_0(k_\parallel) = -2t_0(\cos k_\parallel b - \cos k_\mathrm{F} b), \tag{4}$$

where t_0 is the hopping integral, b is the longitudinal lattice constant, k_F is the Fermi wavenumber, and energy is measured from the Fermi energy.

2.2. Screened interaction

The RPA expression for the screened Coulomb interaction in equation (3) is given by

$$\bar{V}(\mathbf{q}, \omega) = \frac{V(\mathbf{q})}{\varepsilon_m(\mathbf{q}, \omega)}, \tag{5}$$

where

$$V(\mathbf{q}) = \frac{4\pi e^2}{v_0 q^2} \tag{6}$$

is the bare Coulomb interaction with v_0 being the volume of the elementary cell, and

$$\varepsilon_m(\mathbf{q}, \omega) = 1 - V(\mathbf{q})\Pi(\mathbf{q}, \omega) \tag{7}$$

is the corresponding dielectric function. Due to the one-dimensional dispersion (4), the RPA polarization diagram entering into $\varepsilon_m(\mathbf{q}, \omega)$ also depends only on the longitudinal wavenumber,

$$\Pi(\mathbf{q}, \omega) = \Pi(q_\parallel, \omega) = \frac{4}{N_b} \sum_{k_\parallel = -\frac{\pi}{b}}^{\frac{\pi}{b}} \frac{[1 - n(k_\parallel + q_\parallel)] n(k_\parallel) [E_0(k_\parallel + q_\parallel) - E_0(k_\parallel)]}{(\omega + \mathrm{i}\eta \, \mathrm{sgn}\, \omega)^2 - [E_0(k_\parallel + q_\parallel) - E_0(k_\parallel)]^2}. \tag{8}$$

Here N_b is the number of the elementary cells along the chains, and

$$n(k_\parallel) = \begin{cases} 1 & \text{for } E_0(k_\parallel) < 0 \\ 0 & \text{for } E_0(k_\parallel) > 0 \end{cases} \tag{9}$$

is the occupation function at zero temperature.

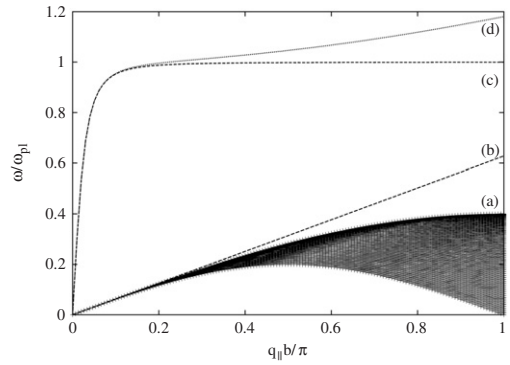

Figure 1. Incoherent and coherent electron–hole excitations for parameters $k_F = \pi/2b$, $t_0 = 0.2$ eV, $\omega_{pl} = 2$ eV, $q_\perp = \frac{1}{10b}$. (a) Incoherent electron–hole range as follows from the polarization diagram (8), (b) the acoustic dispersion line ($\sim v_F q_\parallel$) of its upper part in the long-wavelength limit, (c) the plasmon frequency given by equation (16), and (d) the approximate plasmon dispersion (15).

It is useful for further considerations to look for zeros of the microscopic dielectric function (7) since they determine the energies of electron–hole excitations, dressed due to the Coulomb scattering. In order to distinguish between incoherent dressed electron–hole excitations and collective plasmon ones, we keep the Born–von Karman discreteness of the wavenumbers $k_\parallel, q_\parallel$ in equations (6)–(8),

$$k_i = n_i \frac{2\pi}{L}, \qquad n_i \in Z, \tag{10}$$

where L is a macroscopic length of the sample in the chain direction. Incoherent excitations are those for which the excitation energies $\Omega(k_\parallel, \mathbf{q})$ are *microscopically*, of the order of L^{-1}, close to the energies of the corresponding bare electron–hole excitations with the same wavenumbers,

$$E_0(k_\parallel + q_\parallel) - E_0(k_\parallel) = 4t_0 \sin\frac{2k_\parallel + q_\parallel}{2} b \sin\frac{q_\parallel b}{2}. \tag{11}$$

The energies of incoherent excitations can be determined only in the discrete representation (10) [29], and are represented in figure 1 by a dense set of zeros of $\varepsilon_m(\mathbf{q}, \omega)$ which alternate with its poles at bare electron–hole energies (11).

Collective plasmon excitations have excitation energies which are *macroscopically*, i.e. of the order L^0, far from the edge of the bare electron–hole quasi-continuum shown in figure 1, and therefore can be followed equally well within the continuous approach. Since the plasmon mode will have a central role in the analysis of the electron spectral function, it is useful to simplify its dispersion relation, still keeping all relevant ingredients of the dielectric function, and so enable an analytical treatment of the Dyson equation (3). In the long-wavelength limit $\mathbf{q} \to 0$ the $k_\parallel$-summation in equation (8) reduces to the narrow range $k_F - q_\parallel < k_\parallel < k_F$, and the energy of electron–hole excitations (11) is given by

$$E_0(k_\parallel + q_\parallel) - E_0(k_\parallel) \approx v_F q_\parallel, \tag{12}$$

where $v_F = 2t_0 b \sin k_F b$ is the Fermi velocity. The polarization diagram and the dielectric function then reduce to

$$\Pi(q_\parallel, \omega) \approx \frac{4}{N_b} \frac{v_F q_\parallel^2}{\omega^2 - v_F^2 q_\parallel^2} \frac{L}{2\pi} \tag{13}$$

and

$$\varepsilon_m(\mathbf{q},\omega) = \frac{(\omega + \mathrm{i}\eta\,\mathrm{sgn}\,\omega)^2 - \Omega^2(\mathbf{q})}{(\omega + \mathrm{i}\eta\,\mathrm{sgn}\,\omega)^2 - v_\mathrm{F}^2 q_\parallel^2} \tag{14}$$

respectively. Here

$$\Omega^2(\mathbf{q}) = |q_\parallel|^2 v_\mathrm{F}^2 + \frac{\omega_\mathrm{pl}^2 |q_\parallel|^2}{q^2}, \qquad \omega_\mathrm{pl}^2 \equiv \frac{8e^2 v_\mathrm{F}}{ac} \tag{15}$$

is the dispersion of the collective plasmon mode, with a and c being two perpendicular lattice constants. As is seen from figure 1, the dispersion curve $\Omega(\mathbf{q})$, which is not far from the exact one calculated numerically [30], is much higher than the maximum electron–hole quasi-continuum, even when its value in the long-wavelength regime ($v_\mathrm{F} q_\parallel \to 0$) is extended along the whole first Brillouin zone. For the same reason we can skip the first term in the above expression for $\Omega^2(\mathbf{q})$ and use in further calculations the simplified dispersion

$$\Omega(\mathbf{q}) \approx \omega_\mathrm{pl} \frac{|q_\parallel|}{q} \tag{16}$$

in the whole first Brillouin zone.

2.3. Green's function

We continue by calculating the reciprocal Green's function $G^{-1}(k_\parallel,\omega)$. After performing the ω'-integration it reads

$$\begin{aligned} G^{-1}(k_\parallel,\omega) = \omega - E_0(k_\parallel) + \mathrm{i}\eta[1 - 2n(k_\parallel)] - E_\mathrm{ex}(k_\parallel) - \frac{1}{2N}\sum_{\mathbf{q}} V(\mathbf{q}) \frac{\Omega^2(\mathbf{q}) - v_\mathrm{F}^2 q_\parallel^2}{\Omega(\mathbf{q})} \\ \times \left[\frac{1 - n(k_\parallel + q_\parallel)}{\omega - \mu - \Omega(\mathbf{q}) - E_0(k_\parallel + q_\parallel) + \mathrm{i}\eta} \right. \\ \left. + \frac{n(k_\parallel + q_\parallel)}{\omega - \mu + \Omega(\mathbf{q}) - E_0(k_\parallel + q_\parallel) - \mathrm{i}\eta} \right], \end{aligned} \tag{17}$$

where

$$E_\mathrm{ex}(k_\parallel) = -\frac{1}{N}\sum_{\mathbf{q}} V(\mathbf{q}) n(k_\parallel + q_\parallel) \tag{18}$$

is the exchange energy per elementary cell for the one-particle state with wavenumber $k_\parallel$ [31]. Since $\Omega(\mathbf{q}) \gg v_\mathrm{F} q_\parallel$, the factor $[\Omega^2(\mathbf{q}) - v_\mathrm{F}^2 q_\parallel^2]/\Omega(\mathbf{q})$ in equation (17) can be reduced to $\Omega(\mathbf{q})$. Furthermore, provided that $t_0 \ll \omega_\mathrm{pl}$ the denominators in the $[\cdots]$-brackets can be simplified by neglecting the $q_\parallel$-dependence in the band dispersions $E_0(k_\parallel + q_\parallel)$. The latter step can be justified by noticing that the dependence of $E_0(k_\parallel + q_\parallel)$ on $q_\parallel$ in the denominators is important only for large values of the transverse component $q_\perp \equiv \sqrt{q^2 - q_\parallel^2}$. However, the $\mathbf{q}$-summation in this range gives a negligible contribution to $G^{-1}(k_\parallel,\omega)$ due to the smallness of the factor $V(\mathbf{q})\Omega(\mathbf{q})$. Note also that the ratio ω_pl/t_0 is a measure of the Coulomb interaction strength with respect to the band kinetic energy, and is given by

$$\frac{\omega_\mathrm{pl}^2}{t_0^2} = \frac{64 b^2 \sin k_\mathrm{F} b}{\pi a c} r_s, \tag{19}$$

where b and a, c are longitudinal and transverse lattice constants respectively, and $r_s = r_0/a_0 = \pi/(2k_\mathrm{F} a_0)$ is the longitudinal length per conducing electron normalized by the Bohr radius a_0. Later on we shall discuss the obtained results by choosing for convenience the ratio ω_pl/t_0

in the range 3–4 in order to keep consistency with the above approximations which enable an analytical calculation of $G^{-1}(k_\parallel, \omega)$. Although such choice situates the values of r_s in the range 2–4, i.e. above the strictly perturbational range, these intermediate values of r_s are still small enough with respect to the range of charge localization of Mott type, which indeed does not take place in $(TMTSF)_2X$ salts.

After the above simplifications, the expression (17) reduces to

$$G^{-1}(k_\parallel, \omega) = \omega - E_0(k_\parallel) + i\eta[1 - 2n(k_\parallel)] - E_{ex}(k_\parallel) - \frac{1}{2N}\sum_{\mathbf{q}} V(\mathbf{q})\Omega(\mathbf{q}) \times \left[\frac{1 - n(k_\parallel + q_\parallel)}{\omega - \mu - \Omega(\mathbf{q}) - E_0(k_\parallel) + i\eta} + \frac{n(k_\parallel + q_\parallel)}{\omega - \mu + \Omega(\mathbf{q}) - E_0(k_\parallel) - i\eta}\right]. \tag{20}$$

The chemical potential now follows immediately from the defining condition

$$\mathrm{Re}\, G^{-1}(k_F, \mu) = 0. \tag{21}$$

Taking into account the result (18), we get

$$\mu = -\frac{1}{2N}\sum_{\mathbf{q}} V(\mathbf{q}). \tag{22}$$

The remaining $\mathbf{q}$-integration in equation (20) can be fully performed after approximating the rectilinear first Brillouin zone with the cylinder of the same volume, i.e. that having height $2\pi/b$ and circular base of radius $Q_\perp = 2\sqrt{\pi/(ac)}$, where a and c are the transverse lattice constants. After changing to cylindrical coordinates, and taking into account that $Q_\perp \ll \pi/b$, we get the final expressions for the real and imaginary parts of $G^{-1}(k_\parallel, \omega)$. In the range of frequencies $|\omega - \mu - E_0(k_\parallel)| < \omega_{pl}$ they read

$$\begin{aligned}\mathrm{Re}\, G^{-1}(k_\parallel, \omega) &= \omega - \mu - E_0(k_\parallel) \\ &- \frac{e^2}{2\pi}\left\{\frac{b}{\pi}\frac{Q_\perp^2[\omega - \mu - E_0(k_\parallel)]}{\omega_{pl} - \omega + \mu + E_0(k_\parallel)} + \frac{Q_\perp[\omega - \mu - E_0(k_\parallel)]}{\sqrt{\omega_{pl}^2 - [\omega - \mu - E_0(k_\parallel)]^2}}\right. \\ &\times \ln\left|\frac{\omega_{pl} - \sqrt{\omega_{pl}^2 - [\omega - \mu - E_0(k_\parallel)]^2}}{\omega_{pl} + \sqrt{\omega_{pl}^2 - [\omega - \mu - E_0(k_\parallel)]^2}}\right| + [F_1(k_F - |k_\parallel|, \omega - \mu) \\ &+ F_1(k_F + |k_\parallel|, \omega - \mu)]\Theta\left(\frac{\pi}{b} - |k_\parallel| - k_F\right) + \left[F_1(k_F - |k_\parallel|, \omega - \mu)\right. \\ &\left.\left. + 2F_1\left(\frac{\pi}{b}, \omega - \mu\right) - F_1\left(\frac{2\pi}{b} - k_F - |k_\parallel|, \omega - \mu\right)\right]\Theta\left(k_F + |k_\parallel| - \frac{\pi}{b}\right)\right\},\end{aligned} \tag{23}$$

where

$$\begin{aligned}F_1(x, y) &= 2x\ln|x| - x\ln\left|x^2 - \frac{Q_\perp^2(y - E_0(k_\parallel))^2}{\omega_{pl}^2 - (y - E_0(k_\parallel))^2}\right| \\ &- \frac{Q_\perp(y - E_0(k_\parallel))}{\sqrt{\omega_{pl}^2 - (y - E_0(k_\parallel))^2}}\ln\left|\frac{x + \frac{Q_\perp(y - E_0(k_\parallel))}{\sqrt{\omega_{pl}^2 - (y - E_0(k_\parallel))^2}}}{x - \frac{Q_\perp(y - E_0(k_\parallel))}{\sqrt{\omega_{pl}^2 - (y - E_0(k_\parallel))^2}}}\right|.\end{aligned} \tag{24}$$

The chemical potential and the exchange energy in the expression (23) are given by

$$\mu = -\frac{e^2}{2b}\left\{\frac{2bQ_\perp}{\pi}\arctan\frac{\pi}{bQ_\perp} + \ln\left[\left(\frac{bQ_\perp}{\pi}\right)^2 + 1\right]\right\} \approx -\left(\frac{1}{2}e^2Q_\perp + \frac{e^2}{2\pi^2}Q_\perp^2 b\right) \tag{25}$$

and

$$E_{ex}(k_\parallel) = -\frac{e^2}{2\pi}\left\{\left[F(k_F - |k_\parallel|) + F(k_F + |k_\parallel|)\right]\Theta\left(\frac{\pi}{b} - |k_\parallel| - k_F\right)\right.$$
$$\left. + \left[F(k_F - |k_\parallel|) + 2F\left(\frac{\pi}{b}\right) - F\left(\frac{2\pi}{b} - k_F - |k_\parallel|\right)\right]\Theta\left(k_F + |k_\parallel| - \frac{\pi}{b}\right)\right\} \tag{26}$$

respectively, where

$$F(x) \equiv x\ln(Q_\perp^2 + x^2) + 2Q_\perp \arctan\frac{x}{Q_\perp} - x\ln x^2. \tag{27}$$

The result for the imaginary part of the reciprocal Green's function in the range of frequencies $|\omega - \mu - E_0(k_\parallel)| < \omega_{\rm pl}$ is given by

$$\begin{aligned}\operatorname{Im} G^{-1}(k_\parallel,\omega) = \frac{e^2}{2}\Big\{&2q_c\Theta[\omega_{\rm pl} - \omega + \mu + E_0(k_\parallel)]\Theta[\omega - \mu - E_0(k_\parallel)]\\
&- [\Theta[\omega_{\rm pl} + \omega - \mu - E_0(k_\parallel)]\Theta[-\omega + \mu + E_0(k_\parallel)]\\
&+ \Theta[\omega_{\rm pl} - \omega + \mu + E_0(k_\parallel)]\Theta[\omega - \mu - E_0(k_\parallel)]]\\
&\times\Big[2q_c\Theta(k_{\rm F} - |k_\parallel| - q_c) + 2k_{\rm F}\Theta(q_c - |k_\parallel| - k_{\rm F}) + (k_{\rm F} - |k_\parallel| + q_c)\\
&\times\Theta(|k_\parallel| + q_c - k_{\rm F})\Theta(k_{\rm F} - ||k_\parallel| - q_c|)\Theta\left(\frac{2\pi}{b} - k_{\rm F} - |k_\parallel| - q_c\right)\\
&+\left(2k_{\rm F} + 2q_c - \frac{2\pi}{b}\right)\Theta(k_{\rm F} - ||k_\parallel| - q_c|)\Theta\left(-\frac{2\pi}{b} + k_{\rm F} + |k_\parallel| + q_c\right)\Big]\Big\},\end{aligned} \tag{28}$$

with

$$q_c \equiv \min\left(\frac{|\omega - \mu - E_0(k_\parallel)|Q_\perp}{\sqrt{\omega_{\rm pl}^2 - (\omega - \mu - E_0(k_\parallel))^2}}, \frac{\pi}{b}\right). \tag{29}$$

In the regime $|\omega - \mu - E_0(k_\parallel)| > \omega_{\rm pl}$, we have

$$\operatorname{Im} G^{-1}(k_\parallel,\omega) = 0 \tag{30}$$

and

$$\begin{aligned}\operatorname{Re} G^{-1}(k_\parallel,\omega) = {}&\omega - \mu - E_0(k_\parallel)\\
&- \frac{e^2}{2\pi}\left\{-F_2(\omega - \mu - E_0(k_\parallel)) - \frac{b}{\pi}\frac{Q_\perp^2(\omega - \mu - E_0(k_\parallel))}{\omega_{\rm pl} - \omega + \mu + E_0(k_\parallel)}\right.\\
&+ [F_3(k_{\rm F} - |k_\parallel|, \omega - \mu) + F_3(k_{\rm F} + |k_\parallel|, \omega - \mu)]\Theta\left(\frac{\pi}{b} - |k_\parallel| - k_{\rm F}\right)\\
&+\left[F_3(k_{\rm F} - |k_\parallel|, \omega - \mu) + 2F_3\left(\frac{\pi}{b}, \omega - \mu\right) - F_3\left(\frac{2\pi}{b} - k_{\rm F} - |k_\parallel|, \omega - \mu\right)\right]\\
&\left.\times\Theta\left(k_{\rm F} + |k_\parallel| - \frac{\pi}{b}\right)\right\}\end{aligned} \tag{31}$$

with the same expressions for the chemical potential and exchange energy, while the functions $F_2(x)$ and $F_3(x,\omega)$ are given by

$$F_2(x) = \begin{cases} \dfrac{4xQ_\perp}{\sqrt{x^2-\omega_{\rm pl}^2}}\left[\arctan\left(\sqrt{\dfrac{x+\omega_{\rm pl}}{x-\omega_{\rm pl}}}\,\dfrac{1}{\frac{\pi}{bQ_\perp}+\sqrt{1+(\frac{\pi}{bQ_\perp})^2}}\right)-\arctan\sqrt{\dfrac{x+\omega_{\rm pl}}{x-\omega_{\rm pl}}}\right], \\ \qquad x>\omega_{\rm pl}, \\ \dfrac{4xQ_\perp}{\sqrt{x^2-\omega_{\rm pl}^2}}\left[\arctan\left(\sqrt{\dfrac{|x|+\omega_{\rm pl}}{|x|-\omega_{\rm pl}}}\left(\dfrac{\pi}{bQ_\perp}+\sqrt{1+\left(\dfrac{\pi}{bQ_\perp}\right)^2}\right)\right)\right. \\ \qquad \left.-\arctan\sqrt{\dfrac{|x|+\omega_{\rm pl}}{|x|-\omega_{\rm pl}}}\right], \qquad x<-\omega_{\rm pl}, \end{cases} \tag{32}$$

and

$$F_3(x,y) = 2x\ln|x| - x\ln\left|x^2-\frac{Q_\perp^2(y-E_0(k_\parallel))^2}{\omega_{\rm pl}^2-(y-E_0(k_\parallel))^2}\right| - \frac{2Q_\perp(y-E_0(k_\parallel))}{\sqrt{(y-E_0(k_\parallel))^2-\omega_{\rm pl}^2}}\arctan\left(\frac{x\sqrt{(y-E_0(k_\parallel))^2-\omega_{\rm pl}^2}}{Q_\perp(y-E_0(k_\parallel))}\right), \tag{33}$$

respectively.

Let us look more closely into the functions $\mathrm{Im}\,G^{-1}(k_\parallel,\omega)$ and $\mathrm{Re}\,G^{-1}(k_\parallel,\omega)$ in the range of negative values of $\omega-\mu$, relevant for the photoemission spectra. $\mathrm{Im}\,G^{-1}(k_\parallel,\omega)$ is shown in figure 2. It is seen that $\mathrm{Im}\,G^{-1}(k_\parallel,\omega)\to -e^2k_{\rm F}$ for $\omega\to\mu+E_0(k_\parallel)-\omega_{\rm pl}+0$ and $\mathrm{Im}\,G^{-1}(k_\parallel,\omega)=0$ for $\omega<\mu+E_0(k_\parallel)-\omega_{\rm pl}$. On the other hand, $\mathrm{Im}\,G^{-1}(k_\parallel,\omega)$ vanishes for $k_\parallel<k_{\rm F}$ and $\omega>\mu+E_0(k_\parallel)$, as well as for $k_\parallel>k_{\rm F}$ and $\mu>\omega>\mu-\Omega(k_\parallel-k_{\rm F},Q_\perp)+E_0(k_\parallel)$. The vanishing of $\mathrm{Im}\,G^{-1}(k_\parallel,\omega)$ in the former range, i.e. in the occupied part of the Brillouin zone, can be traced already from the initial equation (20). Namely, for $\omega>\mu+E_0(k_\parallel)$ there are no poles of the bare Green's function with a finite real part, and the poles at $\omega=\mu-\Omega(\mathbf{q})+E_0(k_\parallel)+i\eta$ contribute to $\mathrm{Im}\,G^{-1}(k_\parallel,\omega)$ only in the range $\omega<\mu+E_0(k_\parallel)$. Similarly, for $k_\parallel>k_{\rm F}$ it follows from the expression (20) that due to the presence of the occupation function $n(k_\parallel+q_\parallel)$ the non-vanishing contributions from the dense discrete poles $\omega=\mu-\Omega(\mathbf{q})+E_0(k_\parallel)+i\eta$ of the reciprocal value of the Green's function are possible only for $\omega<\mu-\Omega(k_\parallel-k_{\rm F},Q_\perp)+E_0(k_\parallel)$, i.e. they originate from high-frequency collective excitations. A strict vanishing of $\mathrm{Im}\,G^{-1}$ for $k_\parallel>k_{\rm F}$ in the low-frequency range is in fact the consequence of the exclusion of incoherent excitations from the dielectric function (14). This approximation however does not influence the main conclusions on the properties of $G(k_\parallel,\omega)$ presented below.

A further noticeable feature in figure 2 is a finite plateau in $\mathrm{Im}\,G^{-1}(k_\parallel,\omega)$ at $-e^2k_{\rm F}$ within the energy range $\mu-\omega_{\rm pl}+E_0(k_\parallel)<\omega<\mu-\Omega(\pi/b,Q_\perp)+E_0(k_\parallel)$. It originates from the limitation of the summation in the expression (20) to the range of the first Brillouin zone, $-\frac{\pi}{b}\leqslant q_\parallel\leqslant\frac{\pi}{b}$. Namely, the integration in terms of $q_\perp$ from 0 to $Q_\perp$ in that expression covers poles of $G^{-1}(k_\parallel,\omega)$ in the energy range between $\mu-\omega_{\rm pl}+E_0(k_\parallel)+i\eta$ and $\mu-\Omega(q_\parallel,Q_\perp)+E_0(k_\parallel)+i\eta$, while the subsequent integration in terms of $q_\parallel$ involves only those poles that fulfil the condition $\omega<\mu-\Omega(q_\parallel,Q_\perp)+E_0(k_\parallel)$ for a given value of ω in the range $\mu-\omega_{\rm pl}+E_0(k_\parallel)<\omega<\mu+E_0(k_\parallel)$. The ensuing value for ω, $\omega=\mu-\Omega(q_c,Q_\perp)+E_0(k_\parallel)$, and the requirement that q_c stays in the first Brillouin zone, determine the boundaries $\pm q_c$ of the $q_\parallel$-integration as given by the expression (29). As is seen from this expression, $\frac{|\omega-\mu-E_0(k_\parallel)|Q_\perp}{\sqrt{\omega_{\rm pl}^2-(\omega-\mu-E_0(k_\parallel))^2}}>\frac{\pi}{b}$ for $\mu-\omega_{\rm pl}+E_0(k_\parallel)<\omega<\mu-\Omega(\pi/b,Q_\perp)+E_0(k_\parallel)$, i.e. we have the same boundary $q_c=\frac{\pi}{b}$ of $q_\parallel$-integration for all of these values of ω. The consequence is the plateau in $\mathrm{Im}\,G^{-1}(k_\parallel,\omega)$.

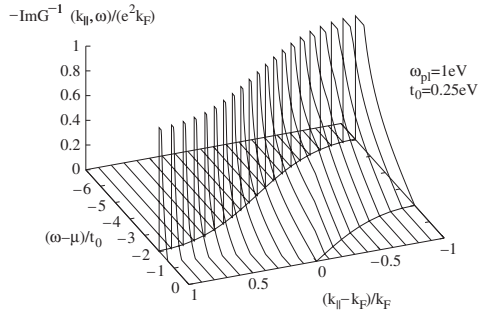

Figure 2. $\mathrm{Im}\, G^{-1}(k_\|, \omega)$ for $k_\mathrm{F} = \pi/2b$. Curves in the $(k_\|, \omega)$-plane represent $E_0(k_\|)/t_0$ and $[E_0(k_\|) - \omega_\mathrm{pl}]/t_0$.

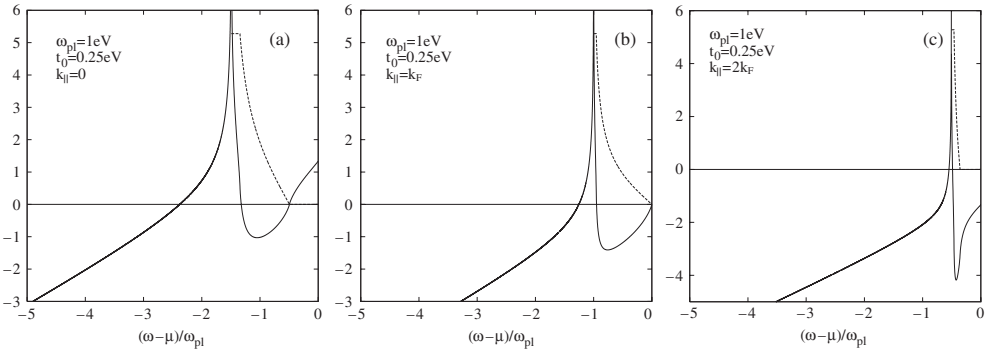

Figure 3. Frequency dependence of $\mathrm{Re}\, G^{-1}(k_\|, \omega)/\omega_\mathrm{pl}$ (full lines) and $-\mathrm{Im}\, G^{-1}(k_\|, \omega)/\omega_\mathrm{pl}$ (dashed lines) for $k_\mathrm{F} = \pi/2b$ and $k_\| = 0$ (a), $k_\| = k_\mathrm{F}$ (b), and $k_\| = 2k_\mathrm{F}$ (c).

The ω-dependence of $\mathrm{Re}\, G^{-1}(k_\|, \omega)$ and $\mathrm{Im}\, G^{-1}(k_\|, \omega)$ is illustrated in figure 3 for three representative values of $k_\|$ ($k_\| = 0, k_\mathrm{F}, 2k_\mathrm{F}$). $\mathrm{Re}\, G^{-1}(k_\|, \omega)$ increases from $-\infty$ as ω increases from $-\infty$, and diverges to $+\infty$ for $\omega = \mu - \omega_\mathrm{pl} + E_0(k_\|) - 0$. At this value of ω, $\mathrm{Im}\, G^{-1}(k_\|, \omega)$ has a step singularity, as was already shown in figure 2. The singularity at $\omega = \mu - \omega_\mathrm{pl} + E_0(k_\|)$ shifts towards larger values of ω as $k_\|$ increases, as is seen in both figures 2 and 3. Furthermore, as $k_\|$ increases, the zero of $\mathrm{Re}\, G^{-1}(k_\|, \omega)$ for $\omega < \mu + E_0(k_\|) - \omega_\mathrm{pl}$ shifts to the right and is closer and closer to the singularity at $\omega = \mu - \omega_\mathrm{pl} + E_0(k_\|)$. As ω further increases from $\omega = \mu - \omega_\mathrm{pl} + E_0(k_\|) + 0$, $\mathrm{Re}\, G^{-1}(k_\|, \omega)$ decreases from $+\infty$, passes through a local minimum, and finally tends towards 0 for $\omega \to \mu + E_0(k_\|)$, in accordance with the expression (23).

It is important to note that $\mathrm{Re}\, G^{-1}(k_\|, \omega)$ has zero in the frequency range $\omega < \mu + E_0(k_\|) - \omega_\mathrm{pl}$ in which $\mathrm{Im}\, G^{-1}(k_\|, \omega)$ also vanishes. Thus we come to the conclusion that only in the range $\omega < \mu + E_0(k_\|) - \omega_\mathrm{pl}$ does the Green's function $G(k_\|, \omega)$ have a first-order pole of the form $\omega_0(k_\|) = E(k_\|) - \mathrm{i}\Gamma(k_\|)$, where $\Gamma(k_\|)$ is infinitesimally small in the present idealized approach, and presumably remains reasonably small (such that $|\Gamma(k_\|)| \ll |E(k_\|)|$) after taking into account usual additional scattering leading to finite relaxations of electronic states. As a consequence, only in this range can the Green's function be expressed in the standard resonant form

$$G(k_\|, \omega) = \frac{Z(k_\|)}{\omega - \omega_0(k_\|)}, \tag{34}$$

where $Z(k_\|) = |\partial\, \mathrm{Re}\, G^{-1}(k_\|, \omega_0(k_\|))/\partial\omega|^{-1}$ is the residuum of the Green's function at the pole $\omega_0(k_\|)$. In other words, quasi-particle excitations exist only for frequencies in the range $\omega < \mu + E_0(k_\|) - \omega_\mathrm{pl}$.

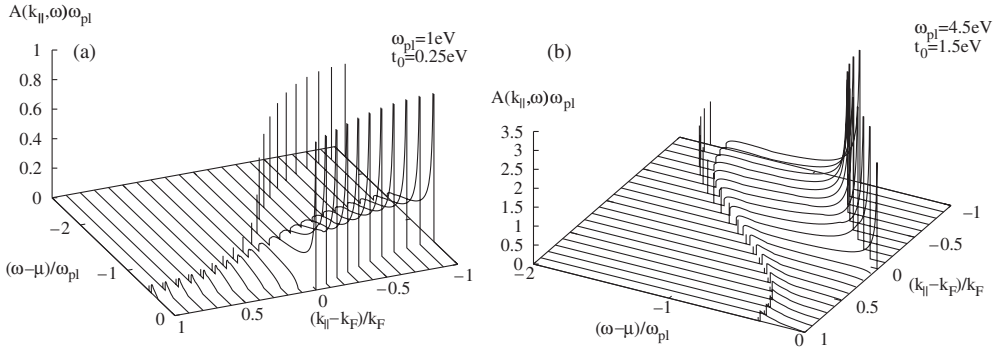

Figure 4. Spectral function $A(k_\parallel, \omega)$ for $\omega_{\rm pl}/t_0$ equal to 4 (a) and 3 (b) in the case $k_{\rm F} = \pi/2b$. Broad maxima for different values of the wavenumber $k_\parallel$ follow from equation (36), while δ-peaks are represented by their weight $Z(k_\parallel)$ according to equation (37).

The above result is qualitatively different from that obtained for the three-dimensional isotropic 'jellium' within the same G_0W_0 approach [21–23]. In the latter case the imaginary part of the reciprocal Green's function vanishes in the frequency range $\mu - \Omega_{\rm pl} < \omega < \mu + \Omega_{\rm pl}$, where $\Omega_{\rm pl}$ is the long-wavelength plasmon frequency. Simultaneously $\mathrm{Re}\, G^{-1}(k_{\rm F}, \omega)$ increases from $-\infty$ for $\omega \to \mu - \Omega_{\rm pl} + 0$ towards ∞ for $\omega \to \mu + \Omega_{\rm pl} - 0$, passing through the zero at $\mu = \omega_0(k_{\rm F})$. Thus the quasi-particle is well defined.

3. Spectral function

The single-particle spectral function

$$A(k_\parallel, \omega) = \frac{1}{\pi} |\,\mathrm{Im}\, G(k_\parallel, \omega)| \tag{35}$$

can be always written in terms of $\mathrm{Re}\, G^{-1}(k_\parallel, \omega)$ and $\mathrm{Im}\, G^{-1}(k_\parallel, \omega)$, namely

$$A(k_\parallel, \omega) = \frac{1}{\pi} \frac{|\,\mathrm{Im}\, G^{-1}(k_\parallel, \omega)|}{[\mathrm{Re}\, G^{-1}(k_\parallel, \omega)]^2 + [\mathrm{Im}\, G^{-1}(k_\parallel, \omega)]^2}, \tag{36}$$

except when $\mathrm{Re}\, G^{-1}(k_\parallel, \omega)$ has a zero $\omega_0(k_\parallel)$ in the frequency range in which $\mathrm{Im}\, G^{-1}(k_\parallel, \omega) = 0$. In the latter case the spectral function is represented by the δ-peak,

$$A(k_\parallel, \omega) = Z(k_\parallel)\delta[\omega - \omega_0(k_\parallel)]. \tag{37}$$

After inserting the results for the real and imaginary parts of reciprocal Green's function $G^{-1}(k_\parallel, \omega)$ given by equations (23)–(30) into (36), (37), we obtain the spectral function as shown in figure 4 for two values of the ratio of plasmon frequency and transfer integral, $\omega_{\rm pl}/t_0 = 3$ and 4. First, the comparison of figures 2 and 4 shows that, apart form the series of high-frequency delta functions, the regions of the non-zero values in $A(k_\parallel, \omega)$ coincide with the corresponding regions of the non-vanishing imaginary part of $G^{-1}(k_\parallel, \omega)$. Furthermore, $A(k_\parallel, \omega)$ has a broad feature at the energy scale of the plasmon energy in the range between $\omega = \mu + E_0(k_\parallel)$ and $\omega = \mu + E_0(k_\parallel) - \omega_{\rm pl}$ which diverges at $\omega = \mu + E_0(k_\parallel)$ for $k_\parallel \leqslant k_{\rm F}$. Note that this range varies slowly with the wavenumber $k_\parallel$. Finally, the spectral weight contains the $k_\parallel$-dependent quasi-particle δ-peak in the energy range $\omega < \mu + E_0(k_\parallel) - \omega_{\rm pl}$.

We point out that the spectral function presented above obeys excellently the sum rule

$$\int_{-\infty}^{\infty} A(k_\parallel, \omega)\, \mathrm{d}\omega = 1, \tag{38}$$

the numerical agreement being better than 10^{-2} in the whole range of the wavevector $k_\parallel$, and for all investigated values of the ratio $\omega_{\rm pl}/t_0$.

The behaviour of the spectral function in figure 4 is to be contrasted to that of three-dimensional isotropic normal metals. In the latter case the reciprocal Green's function is analytical at the Fermi wavenumber $k_{\rm F}$ and in the vicinity of $\omega = \mu$, so the Landau theory of Fermi liquids can be applied. As is explicitly shown within the G_0W_0 approximation for the 'jellium' model [21–23], the spectral function then has a quasi-particle δ-peak at μ for $k_\parallel = k_{\rm F}$. In the actual case of a quasi-one-dimensional metal the Landau theory of Fermi liquids cannot be applied due to the existence of the low-energy collective modes which introduce singularities of the reciprocal Green's function in the vicinity of $\omega = \mu$ and for $k_\parallel = k_{\rm F}$. These singularities are the direct consequence of the anisotropy of the plasmon dispersion (16), i.e. of its acoustic nature with $\omega_{\rm min} = 0$, which leads to the formation of the broad feature in the spectral function. The form of $A(k_\parallel, \omega)$ shown in figure 4 is qualitatively in agreement with ARPES experiments on some quasi-one-dimensional conductors [5–7] which also show broad structures and the absence of low-energy quasi-particle peaks in the spectral functions.

Let us now look more closely into the spectral function (36) for $k_\parallel = k_{\rm F}$ and in the limit $\omega \to \mu^-$. Since for $\omega \approx \mu$

$$\mathrm{Re}\, G^{-1}(k_{\rm F}, \omega) \approx \omega - \mu - \frac{e^2}{2\pi}\left[\frac{Q_\perp(\omega-\mu)}{\omega_{\rm pl}} \ln\left(\frac{(\omega-\mu)^2}{2\omega_{\rm pl}^2}\right) + \frac{b}{\pi} Q_\perp^2 \frac{\omega-\mu}{\omega_{\rm pl}}\right], \tag{39}$$

$$\mathrm{Im}\, G^{-1}(k_{\rm F}, \omega) = -\frac{e^2}{2} \frac{|\omega-\mu| Q_\perp}{\sqrt{\omega_{\rm pl}^2 - (\omega-\mu)^2}}, \tag{40}$$

the spectral function then reads

$$A(k_{\rm F}, \omega) \approx \frac{e^2}{2\pi} \frac{Q_\perp}{|\omega-\mu|\omega_{\rm pl}\left[1 - \frac{e^2}{2\pi}\frac{Q_\perp}{\omega_{\rm pl}}\left(\ln\left(\frac{(\omega-\mu)^2}{2\omega_{\rm pl}^2}\right) + \frac{b}{\pi} Q_\perp\right)\right]} \tag{41}$$

and diverges for $\omega \to \mu$. The absence of quasi-particle δ-functions in the spectral function is the consequence of the fact that the ω-dependence of $\mathrm{Im}\, G^{-1}(k_{\rm F}, \omega)$ differs from the quadratic law which is the essential property of Fermi liquids. Also, our expression (41), obtained within the G_0W_0 approximation, differs from the corresponding expression for the spectral function in the one-dimensional spinfull spin-rotation-invariant Luttinger model obtained within an exact bosonization treatment [4],

$$A(k_{\rm F}, \omega) \sim |\omega - \mu|^{\alpha-1}, \tag{42}$$

where $\alpha = (K_\rho + K_\rho^{-1} - 2)/4$ is the anomalous dimension, with the 'charge stiffness constant' given by $K_\rho = \sqrt{\frac{\pi v_{\rm F} + g_{4\rho} - g_{2\rho}}{\pi v_{\rm F} + g_{4\rho} + g_{2\rho}}}$, where $g_{2\rho}$ and $g_{4\rho}$ are coupling constants for the forward Coulomb scattering in the charge sector.

Let us recall here that in the Luttinger model the eigenstates of the system are long-range charge and spin acoustic collective modes, obtained as combinations of the low-energy electron–hole excitations, while low-energy quasi-particles are not present. The result (42) for α exceeding unity would be in agreement with the results of the photoemission experiments on quasi-one-dimensional metals [5–7] in the low-energy range, provided that the latter are indeed microscopically relevant. This would be an indication that these materials belong to the regime of the strong long-range interaction within the Luttinger model, as was also concluded in the theoretical analyses in [12, 32, 33].

Let us also mention for the sake of completeness that ARPES spectra of the quasi-two-dimensional crystals in the normal conducting phase show the quasi-particle at the chemical

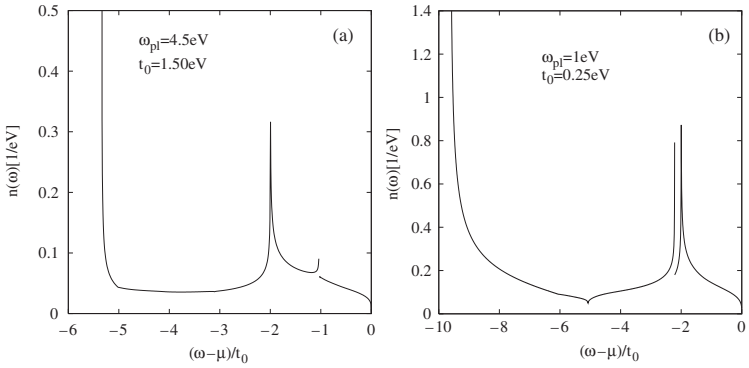

Figure 5. Density of states $n(\omega)$ for $\omega_{\rm pl}/t_0$ equal to 3 (a) and 4 (b), and for $k_{\rm F} = \pi/2b$.

potential superimposed to the broad hump at higher energies [34]. A spectral function with such properties was obtained by Artemenko *et al* [35] who studied the RPA screening of Coulomb interaction in the model of a quasi-two-dimensional metal with the metallic planes connected by the finite perpendicular overlap integral $t_\perp$. In this model the collective mode has a spectrum with a finite minimum $\omega_{\rm min} \neq 0$ due to the finiteness of the overlap integral $t_\perp$.

4. Density of states and momentum distribution

Let us first consider the density of states

$$N(\omega) = \sum_{\mathbf{k}} A(k_\parallel, \omega) \tag{43}$$

where the **k** summation goes over the same first Brillouin zone as before. After changing to cylindrical coordinates and integrating in terms of $k_\perp$, the density of states per number of electrons in the system reads

$$n(\omega) \equiv N(\omega)/N_e = \frac{1}{2k_{\rm F}} \int_0^{\frac{\pi}{b}} A(k_\parallel, \omega)\, {\rm d}k_\parallel, \tag{44}$$

where $N_e \equiv 2(2k_{\rm F}\frac{4\pi^2}{ac})/(8\pi^3/V)$. After integrating the spectral density $A(k_\parallel, \omega)$ numerically, we arrive at the result for $n(\omega)$ shown in figure 5 for the values of the ratio $\omega_{\rm pl}/t_0$ equal to 3 and 4 as in figure 4. The density of states falls from the maximum value in the range of negative energies to the local minimum, and then rises to the discontinuity which can be of two types. First, if the highest energy of the $k_\parallel$-dependent quasi-particle δ-peak in the energy range $\omega < \mu + E_0(k_\parallel) - \omega_{\rm pl}$ is less than $\mu + E_0(k_\parallel)$, there is a step discontinuity at this energy, as is shown in the figure 5(b) for $\omega_{\rm pl}/t_0 = 4$. As ω further increases the density of states increases and diverges to $+\infty$ at $\mu + E_0(k_\parallel)$, and then continuously falls to zero at $\omega = \mu$. Second, if the highest energy of the $k_\parallel$-dependent quasi-particle δ-peak in the energy range $\omega < \mu + E_0(k_\parallel) - \omega_{\rm pl}$ is greater than $\mu + E_0(k_\parallel)$, the density of states diverges at $\mu + E_0(k_\parallel)$. As ω further increases it falls to the local minimum and rises to a step discontinuity at the highest energy of the $k_\parallel$-dependent quasi-particle δ-peak in the energy range $\omega < \mu + E_0(k_\parallel) - \omega_{\rm pl}$, as is shown in figure 5(a) for the case $\omega_{\rm pl}/t_0 = 3$. Finally, as ω further increases, the density of states falls to zero at $\omega = \mu$.

It is instructive to compare the above G_0W_0 result for the density of states with the density of states for the non-interacting electron band having the tight-binding dispersion (4),

$$n_0(\omega) = \frac{1}{2k_{\rm F}} \int_0^{\frac{\pi}{b}} \delta(\omega - E_0(k_\parallel))\, {\rm d}k_\parallel = \frac{1}{4k_{\rm F}t_0 b|\sin k_{\parallel 0}|}, \tag{45}$$

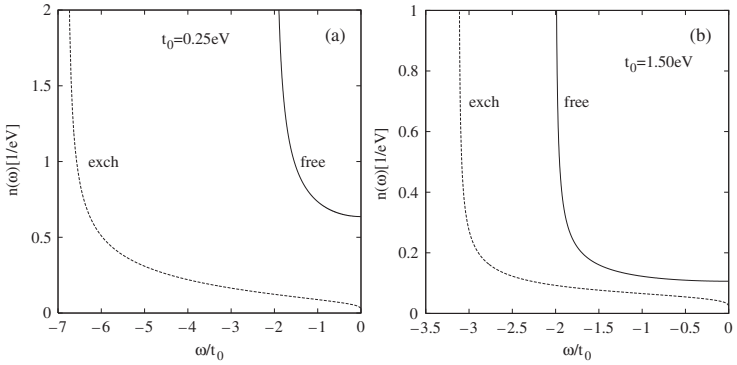

Figure 6. Density of states of the tight-binding band and the 'exchange' density of states obtained by taking into account only the exchange contribution (26) to the spectral function (44) measured from the corresponding chemical potentials, for $k_F = \pi/2b$ and $t_0 = 0.25$ eV (a) and 1.5 eV (b).

where $k_{\|0}$ is the zero of the equation $\omega - E_0(k_{\|0}) = 0$. As shown in figure 6, this free-particle density of states diverges at the edges of the electron band (4), and has a minimum equal to $1/(4k_F t_0 b)$ in the middle of the band ($\omega = 0$). In the same figure we show for comparison the density of states obtained after taking into account only the exchange energy (26) in the Green's function (17). The exchange contribution itself shifts the chemical potential to the negative value $E_{ex}(k_F)$. The density of states measured from this chemical potential is shifted to negative energies that exceed the bandwidth. The rest of the G_0W_0 self-energy shifts the density of states even more to negative energies with respect to the G_0W_0 chemical potential μ, giving noticeable gain at energies of the order of the plasmon energy, as is shown in figure 5.

Such behaviour differs from the corresponding behaviour of the density of states in the Luttinger model which has potential behaviour at low energies [4]

$$N(\omega) \sim |\omega - \mu|^{\alpha}, \tag{46}$$

where α is the interaction-dependent anomalous dimension from equation (42), and contains a maximum at a finite energy. This maximum guarantees the fulfilment of the sum rule, but its position cannot be directly scaled with the band width or the plasmon energy due to the irrelevance of the energetic cut-off choice in the bosonization procedure applied to the Luttinger model. In contrast to that, the present G_0W_0 calculation shows that the broad feature with the divergence at $\mu + E_0(k_{\|})$ in the density of states takes place at energies of the order of the plasmon energy.

We are now in position to calculate the momentum distribution function

$$n(k_{\|}) = \int_{-\infty}^{\mu} A(k_{\|}, \omega)\, \mathrm{d}\omega, \tag{47}$$

and to check the self-consistency of the G_0W_0 approximation. The results of the numerical calculation are shown in figure 7, again for the same values of the ratio ω_{pl}/t_0 as in previous figures. We find that the areas below curves (a) and (b) differ from the exact number of electrons by less than 4% and 9% respectively. This result proves that the G_0W_0 approximation is satisfactorily self-consistent.

The form of the momentum distribution function from figure 7 indicates that there are no low-energy quasi-particles in the dressed electron spectrum. Furthermore, the curves for $n(k_{\|})$ have divergent derivations at $k_{\|} = k_F$, which is also a property of Luttinger liquids [36]. On the other hand, the G_0W_0 approximation in the case of a three-dimensional isotropic 'jellium'

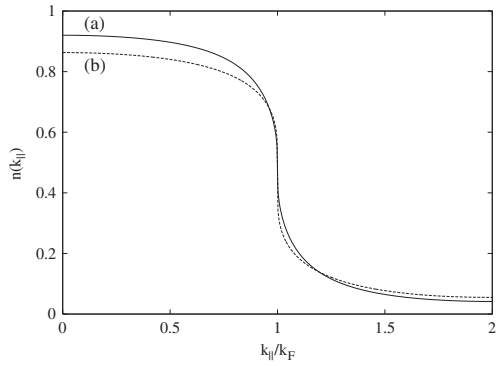

Figure 7. Momentum distribution function for $k_F = \pi/2b$ and ω_{pl}/t_0 equal to 4 (a) and 3 (b).

shows a typical Fermi liquid behaviour, i.e. $n(k_\parallel)$ has a finite discontinuity at $k_\parallel = k_F$ equal to the spectral weight of the quasi-particle at k_F [21, 22].

Our preliminary considerations of the extension of the present treatment to the range of finite transverse bandwidths show that the finite transverse bandwidth is responsible for the appearance of an optical gap in the plasmon mode [19, 20]. Plasmon dispersion of such a kind in turn introduces into the spectral function the quasi-particle δ-peak at the chemical potential, in agreement with the results of [33] obtained in a different approach. In this way one can follow continuously how the electron spectral properties vary as one passes from the highly anisotropic (quasi-one-dimensional) limit to the fully isotropic one. Experimentally, 'weak' quasi-particles in the regime of small transverse bandwidths are still not detected.

5. Conclusion

Although, as discussed in the previous section, our G_0W_0 expression for the spectral function does not reproduce the exact result obtained before for Luttinger liquids in the asymptotic low-frequency regime, we expect that it gives a qualitatively good description of the spectral properties of quasi-one-dimensional conductors at the energy scale of the plasmon energy. Our analysis shows that the strongly anisotropic low-frequency plasmon modes induced by the long-range Coulomb interaction in the conducting electron band with a (quasi)-one-dimensional dispersion give a dominant contribution to the electron self-energy, and are responsible for the electronic spectral properties in the normal phase.

More precisely, the acoustic plasmon anisotropy causes the formation of the broad feature at the energy scale of the plasmon frequency. Simultaneously the quasi-particle δ-peaks and the corresponding spectral weight shift to higher energies. The broad feature loses its spectral weight relatively with respect to the contributions from the quasi-particle δ-peaks as the ratio of the plasmon energy to the hopping integral in the chain direction increases. Furthermore, the broad feature depends weakly on the wavevector $k_\parallel$, this dependence being weaker and weaker with respect to the dispersion of the quasi-particle δ-peaks as the ratio of the plasmon energy to the hopping integral in the chain direction increases. Such behaviour of the spectral function is in qualitative agreement with the ARPES spectra obtained for some Bechgaard salts.

The disappearance of low-energy quasi-particle excitations in the spectral function is the central result of the present calculation, which shows that already at the G_0W_0 stage the spectral properties of the quasi-one-dimensional band differ qualitatively from those for three-dimensional isotropic normal metals showing standard Fermi liquid properties. Comparing these two results, we come to the conclusion that due to the existence of the low-energy

collective modes of quasi-one-dimensional metals, the standard starting point of the Fermi liquid approach, namely the expansion of the Green's function around the Fermi energy, is not allowed. On the other hand, the present G_0W_0 approach enables the determination of the position of the broad feature in the spectral function, in contrast to the Luttinger liquid approach, which is limited to the exact determination of the power law behaviour in the low-frequency region. The two methods can be thus considered as complementary in the analysis of the role of collective modes in the spectral properties of the quasi-one-dimensional conductors, giving an overall complete insight in the wide energy range relevant for ARPES measurements.

Acknowledgment

The work is supported by the Croatian Ministry of Science, Education and Sport, through project no. 0119251.

References

[1] Abrikosov A A, Gorkov L P and Dzyaloshinski I E 1975 *Methods of Quantum Field Theory in Statistical Physics* (New York: Dover)
[2] Luttinger J M and Ward J C 1960 *Phys. Rev.* **118** 1417
[3] Luttinger J M 1960 *Phys. Rev.* **119** 1153
[4] Voit J 1993 *J. Phys.: Condens. Matter* **5** 8305
[5] Zwick F *et al* 1997 *Phys. Rev. Lett.* **79** 3982
[6] Zwick F *et al* 2000 *Solid State Commun.* **113** 179
[7] Zwick F *et al* 2000 *Eur. Phys. J.* B **13** 503
[8] Sing M *et al* 2003 *Phys. Rev.* B **67** 125402
[9] Barišić S 1983 *J. Physique* **44** 185
[10] Schulz H J 1983 *J. Phys. C: Solid State Phys.* **16** 6769
[11] Botrić S and Barišić S 1984 *J. Physique* **45** 185
[12] Kopietz P, Meden V and Schönhammer K 1995 *Phys. Rev. Lett.* **74** 2999
[13] Bourbonnais C 1993 *J. Physique* I **3** 143
[14] Wzietek P *et al* 1993 *J. Physique* I **3** 171
[15] Vescoli V *et al* 1998 *Science* **281** 1181
[16] Schwartz A *et al* 1998 *Phys. Rev.* B **58** 1261
[17] Giamarchi T 1997 *Physica* B **230–232** 975
[18] Auban-Senzier P, Jérome D and Moser J 1999 *Physical Phenomena at High Magnetic Fields* ed Z Fisk, L P Gorkov and J R Schrieffer (Singapore: World Scientific) p 211
[19] Agić Ž, Županović P and Bjeliš A 2004 *J. Physique* IV **114** 95
[20] Bonačić Lošić Ž, Županović P and Bjeliš A 2006 *PhD Thesis* University of Zagreb
[21] Hedin L and Lundqvist S 1969 *Solid State Physics* vol 23, ed F Seitz, D Turnbull and H Ehrenreich (New York: Academic) p 1
[22] Lundqvist B I 1967 *Phys. Kondens. Mater.* **6** 206
[23] Lundqvist B I 1968 *Phys. Kondens. Mater.* **7** 117
[24] García-Gonzáles P and Godby R W 2001 *Phys. Rev.* B **63** 075112
[25] Schindlmayr A 1997 *Phys. Rev.* B **56** 3528
[26] Hedin L 1965 *Phys. Rev.* **139** A796
[27] Doniach S and Sondheimer E H 1974 *Green's Functions for Solid State Physicists* (Reading, MA: Benjamin)
[28] Fetter A L and Walecka J D 1971 *Quantum Theory of Many Particles* (New York: McGraw-Hill)
[29] Županović P, Bjeliš A and Agić Ž 2001 *Fizika A (Zagreb)* **10** 203
[30] Williams P F and Bloch A N 1974 *Phys. Rev.* B **10** 1097
[31] Mahan G D 2000 *Many Particle Physics* (New York: Kluwer–Academic)
[32] Meden V and Schönhammer K 1992 *Phys. Rev.* B **46** 15753
[33] Kopietz P, Meden V and Schönhammer K 1997 *Phys. Rev.* B **56** 7232
[34] Dessau D S *et al* 1993 *Phys. Rev. Lett.* **71** 2781
[35] Artemenko S N and Remizov S V 2001 *JETP Lett.* **74** 392 (*Preprint* cond-mat/0109264)
[36] Meden V 1999 *Phys. Rev.* B **60** 4571